Acta Geophysica (2023) 71:1321–1334
https://doi.org/10.1007/s11600-022-01014-z

RESEARCH ARTICLE - ATMOSPHERIC & SPACE SCIENCES

Performance of the Indian summer monsoon 2020 in NCEP-GFS

Pemmani Venkata Subba Raju[1] · Akshay Kulkarni[1] · Muhammed Muhshif Karadan[1] · Dongxiao Wang[2]

Received: 8 August 2022 / Accepted: 30 December 2022 / Published online: 23 January 2023

Abstract
The rainfall observed 957.6 mm during summer monsoon season (June–September) of 2020 over India, which is 9% more than the climatological mean summer monsoon rainfall. In this study, the Indian Summer Monsoon (ISM) features are evaluated with National Center for Environment Prediction-Global Forecast System (NCEP-GFS). The 1200 UTC operational analysis and forecast fields (up to 5 days) with 0.5° horizontal resolution and 64 vertical levels are archived for the period of 1st May up to 30th September 2020. The ISM characteristics such as the low-level westerly jet at 850 hPa throughout the monsoon season, reaching the maximum intensity (> 18 m sec^{-1}) on the Somalian coast and upper-level tropical easterly jet at 150 hPa (> 30 m sec^{-1}) are well reflected in the NCEP analysis during summer monsoon season. The NCEP model reveals that the ISM features are reasonably well predicted in day 1 forecast, whereas in day 3 and day 5 forecasts it exhibited certain biased tendencies with respect to NCEP analysis. The spatial distribution of observed rainfall was in good agreement with the day 1, day 3, and day 5 forecasts; however, the intensity was overestimated over central India when compared to India Meteorological Department (IMD) observations. The heavy rainfall events (> 64.5 mm as per the criteria of IMD) were realistically captured in the day 1 forecast in terms of spatial distribution and intensity, but the model has limitations to capture intensity and distribution on day 3 and day 5 forecasts.

Keywords Indian summer monsoon · NCEP analysis and forecast · Westerly jet · Tropical easterly jet

Introduction

The south-west monsoon season exhibits major changes over India, influencing the country's rainfall pattern. The intensity and duration of rainfall are associated with semi-permanent systems such as Mascarene high, low-level westerly flow, upper tropical easterly winds, heat-low over north-west India, Tibetan anticyclonic circulation, monsoon depressions, and troughs over the Indo-Gangetic plain during the monsoon season (Webster et al. 1998; Mohanty et al. 2005). The meridional pressure gradient along with the Coriolis force between the Indo-Gangetic plain and Mascarene island of Indian Ocean enhance the cross-equatorial circulation (Krishnan et al. 2020). Moisture is transported into the Indian subcontinent through cross-equatorial flow across the Somalia coast and a westerly low-level jet (LLJ) at 850 hPa over the Arabian Sea (AS), which is heavily accompanied by rainfall over this region (Mohanty et al. 2003; Raju et al. 2005; Wang et al. 2009). In addition to the low-level circulation, during the monsoon season there also exist an active upper-level circulation called tropical easterly jet (TEJ) at a pressure level of 200 hPa (Karadan et al. 2021). A decreased mean sea level pressure is also observed over the north-western India during the entire monsoon season called heat-low. Furthermore, an anticyclonic circulation presenting over the south-east of Tibet at upper level also characterizes the monsoon by assisting the TEJ by its equatorward outflows (Raghavan 1973). The monsoon rainfall distribution in India is determined by the movement in the monsoon trough over the Himalayan foothills (Mohanty et al. 2003; Rao et al. 2003). The unprecedented breaks in the rainfall during the monsoon season may lead to a drought situation over India, thereby affecting various sectors (Gadgil et al. 2005; Raju et al. 2010). Therefore, from the onset through the advance of monsoon till its withdrawal

Edited by Prof. Ioannis Pytharoulis (ASSOCIATE EDITOR) / Prof. Theodore Karacostas (CO-EDITOR-IN-CHIEF).

✉ Pemmani Venkata Subba Raju
pemmani@gmail.com; pvsraju@jpr.amity.edu

[1] Centre for Ocean Atmospheric Science and Technology, Amity University Rajasthan, Kant Kalwar, Jaipur, India

[2] South China Sea Institute of Oceanology, Chinese Academy of Sciences, 164 West Xingang Road, Guangzhou, China

from the region, monsoon traverse through various active and break spells determining the nature of its seasonal rainfall intensity. This strong regional climate system directly or indirectly influence the life and their livelihoods of 1.6 billion residents of South Asia (Ashfaq et al. 2021). A moderate to normal rainfall provides the region with good agricultural yields, whereas the extreme excess rainfall or drought season makes the living circumstances more miserable (Patwardhan et al. 2014).

Several national and international institutions use General Circulation Models (GCM) for seamless weather and climate scale forecast (Pattanaik and Kumar 2010; Pattanaik et al. 2020). Further, the GCM output is used in mesoscale models to generate high-resolution simulations/forecasts over the region (Kumar et al. 2017). These models tend to drift towards their ideal climatology as the forecast period lengthens, and this tendency causes bias in predictions (Heckley 1985; Arpe and Klinker 1986; Acharya et al. 2012). The diagnosis of the source of these errors associated with the simulation/prediction of the Indian Summer Monsoon (ISM) region is a vital part of the refinement of prediction models. The major contributions of these inaccuracies in the numerical models can be attributed to the improper representation of sub-grid scale physical processes such as planetary boundary layer, cumulus convection, radiation, land surface processes, and their complex interactions (Saha et al. 2014; Raju et al. 2022). The empirical data (initial condition) inaccuracy in the model could also contribute to the forecast error (Pokhrel et al. 2016; Wang et al. 2018). Therefore, the evaluation of these errors along with assessing the forecast skill of the GCMs is required over the ISM to improve the forecast skill (Wang et al. 2005). Although most of these models are capable of simulating the regional monsoon characteristics, the intensity and distribution differ in each model (DelSole and Shukla 2012). Therefore, an efficient approach is vital to determine the skill of the GCM. In this paper, we aim to address the following aspects.

- Investigating summer monsoon 2020 features over India with observation and National Centers for Environment Prediction (NCEP) analysis.
- Assessing the forecast ingenuity of NCEP for the prediction of summer monsoon features in day 1, day 3, and day 5.
- Examining the extreme weather episode during the ISM season over India in NCEP analysis and forecasts.

Synoptic features of monsoon 2020

The south-west monsoon arrived over the Andaman Sea on 17th May and set over Kerala on 1st June 2020. The commencement of ISM 2020 was associated with a cyclonic system (Nisarga) over the eastern AS. It intensified into a severe cyclonic storm and moved north to north-eastward, crossing the Maharashtra coast on 3rd June. The monsoon advanced and engulfed the whole country on 26th June which was 12 days earlier than the normal date. In addition to the cyclonic system over the AS, a low-pressure cyclonic movement over the west-central Bay of Bengal (BoB) strengthened the monsoon flow and reinforced the progression of the monsoon over the country. During the summer monsoon season, 12 low-pressure systems were observed of which five systems were formed in August. This triggered the monsoon activity, shifting the active monsoon trough towards the south of its regular position, and it maintained a strong low-level westerly jet around the AS. This significantly further enhanced the precipitation over the central and western parts of India. The presence of a low-pressure system during the 1st week of August caused heavy rainfall which led to a flood situation over Gujarat and the coastal regions of Maharashtra. The uncommon shifting of the monsoon trough to the Himalayan foothills made the July month deficient (by 10%) in rainfall over southern parts of India. This trough triggered floods over north-eastern India, Bihar, and Uttar Pradesh. The formation of two low-pressure systems in September led to an active monsoon delaying the withdrawal. The departure of the monsoon only began on 28th September from western Rajasthan and Punjab which is quite far from its normal date of 17th September. The season (June–September) in 2020 in India recorded 957.6 mm of rainfall which is 9% above its long-period average (LPA). The seasonal rainfall recorded over four homogeneous regions, namely north-west India, central India, southern peninsular India, and north-eastern India, respectively, are − 16%, + 15%, + 30%, and + 6% of their corresponding LPA (Mausam 2021).

The ENSO and IOD patterns strongly influence the ISM rainfall. Sea surface temperature (SST) anomalies are reported in order to better understand the evolution of SST over the Pacific and Indian Oceans as it affects large-scale circulation and monsoonal patterns, as well as their state prior to and during monsoon season. The monthly SST anomalies from April to September and the daily variation of area-averaged Nino3.4, Western Equatorial Indian Ocean (WEIO) and Eastern Equatorial Indian Ocean (EEIO) are shown in Fig. 1a–g (Source: https://psl.noaa.gov/data/gridded/data.noaa.oisst.v2.highres.html). Over the equatorial Pacific Ocean, SST positive anomalies reveal the onset of El Nino conditions from May to September, whereas in the Indian Ocean, a weak positive Indian Ocean Dipole (IOD) during the onset of monsoon, which then turned neutral in July, and then a negative IOD until September. During May and June, the area-averaged SST over WEIO and EEIO have an inverse relationship with warmer EEIO seas and colder WEIO waters (negative IOD phase). Furthermore, during August and September, a negative

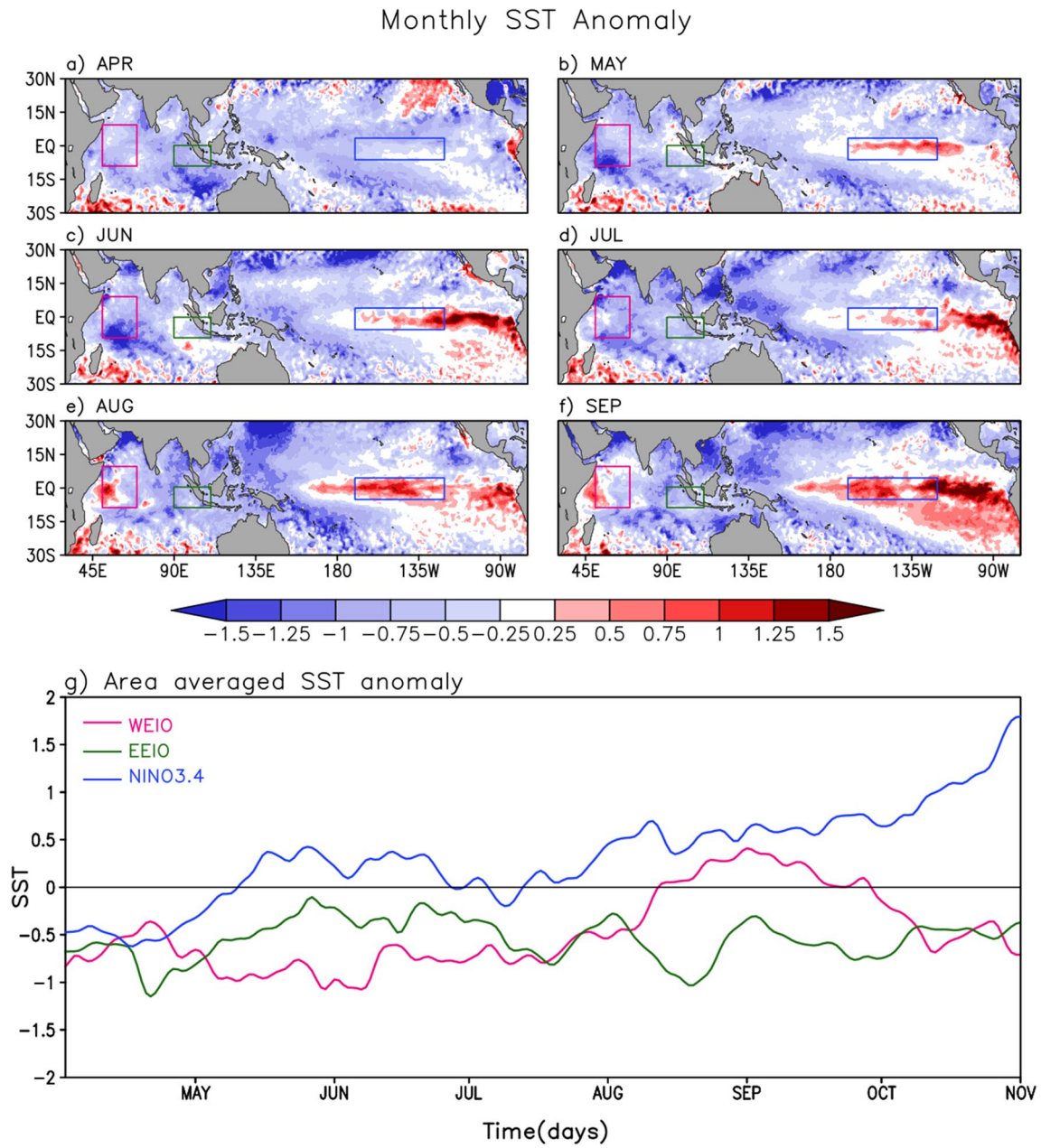

Fig. 1 Monthly spatial pattern of SST anomaly (**a**–**f** and **g**) area average time series over Nino3.4 and IOD regions (**g**). (*Source* NOAA OI SST V2 High Resolution Dataset)

SST anomaly over EEIO denotes a positive IOD (Fig. 1g). At the same time, the temperature anomaly over the Nino3.4 region shifts from negative to positive, signalling the onset of El Nino (Kug et al. 2010).

Methods and materials

The Global forecasting system (GFS) is a non-hydrostatic finite volume cubed sphere (FV3) dynamic global model (Kanamitsu 1989; Kanamitsu et al. 1991; Kalnay et al. 1996; Putman and Lin 2007). The NCEP GFS contains a finite volume cubed sphere dynamical core that was enhanced by NOAA's Office of Atmospheric Research's Geophysical Fluid Dynamics Laboratory (GFDL) (OAR). In terms of its dynamical core and physics, the present operational GFS model has undergone significant alterations since 1996. Modifications to physics packages include advanced GFDL microphysics, improved parameterization of middle atmospheric water vapour photochemistry, a modified convective parameterization scheme to reduce excessive cloud-top cooling, and an updated bare soil evaporation scheme

(Lin 2004). GFS runs up to 16 days at various horizontal resolutions (0.25°, 0.5°, 1.0°, and 2.5°), with 64 vertical levels daily four times (0000, 0600, 1200, 1800 UTC) in real-time operational mode at the NCEP and its outputs are available for public. These model outputs are widely employed for operational purposes as well as further dynamical downscaling for localized applications by diverse organizations across the world.

In this study, NCEP GFS analysis at 1200UTC and model forecast of day 1, day 3, and day 5 data with a resolution of $0.5° \times 0.5°$ are used to diagnose the ISM season of 2020. The observed rainfall gridded data (0.25°) were archived from India Meteorological Department (IMD). The observed ISM characteristics of the year 2020 across South Asia were analysed with observed and NCEP analysis. For four homogeneous locations, the monthly geographical distribution and daily accumulated rainfall were examined. In addition, the model's ability to predict wind, temperature, specific humidity, and geopotential height for day 1, day 3, and day 5 in South Asia was assessed and compared to analysis fields. The 24-h accumulated precipitation for day 1, day 3, and day 5 forecast during monsoon season has been compared with IMD gridded rainfall data (Mitra et al. 2009). Furthermore, NCEP analysis and forecast fields were used to investigate excessive precipitation linked with tropical cyclones during the onset of the monsoon, as well as heavy rainfall occurrences.

Results and discussion

Observed features of summer monsoon 2020

The spatial distribution of observed monthly gridded precipitation with a resolution of 0.25° archived from IMD during the summer monsoon of 2020 is exhibited in Fig. 2a–d. The monthly rainfall distribution follows a typical climatological trend, with the western coast, central, and north-east Indian regions receiving the most rain. In the first week of June, cyclone Nisarga made landfall on Maharashtra's south-west coast, causing torrential rains as shown in Fig. 2a–c. As a result of severe cyclonic storm Nisarga coinciding with the onset of the summer monsoon, maximum rainfall was recorded across the west coast and north-east of the AS Fig. 2a.

In June (Fig. 2a), as the monsoon arrived in central India, there was widespread rain across the country. The northern section of India had less rain in June than the eastern part, but both received sufficient rainfall. Northern India had been covered by the Northern Limit of Monsoon (NLM) by the end of June, and significant rainfall was recorded along the Himalayan foothills. In July (Fig. 2b), north-east India received the most rainfall, resulting in floods in Bihar and Assam. This could be due to a shift in the monsoon trough's northward progression. Coastal and central India experienced less rainfall in July due to the lack of major systems in the BoB. Northern BoB and central India received excessive rainfall in August (Fig. 2c), which was accompanied by a large number of monsoon depressions over BoB. Furthermore, due to a stronger low-level westerly jet over the AS, heavier rainfall was seen along the west coast and in Gujarat. The delay in the withdrawal of the monsoon (28th September) was caused due to the formation of low-pressure circulations over BoB in September (Fig. 2d), which enhanced precipitation over the central and southern peninsular India, whereas north and north-west India noticed a reduction in rainfall.

Figure 3 depicts observed daily accumulated rainfall over four homogenous regions in India from June to September. The maximum rainfall was clearly displayed in the southern peninsular area during the first week of June, which was also related to the severe cyclonic storm Nisarga. The active rain spell occurs in the first part of August, with break-type conditions occurring in the second half of the month. Overall, rainfall in the South Indian peninsular region was 30% more than the mean rainfall climatology (Fig. 3d). The central Indian region receives the most rainfall in August, although the same region receives significantly less rainfall in July. The central Indian region recorded 15% above normal rainfall from June to September (Fig. 3c). Over the north-west region (Fig. 3b), July and August received normal rainfall, whereas June and September perceive deficit rainfall that leads to 15% below average rainfall for the whole season. Peak rainfall occurrences in north-east India in the first half of July and the second half of September demonstrate the region's heavy rainfall events (Fig. 3a).

Monsoon features in NCEP analysis

The spatial distribution of wind at lower and upper atmospheric levels for the pre-monsoon and monsoon seasons of 2020 is represented in Fig. 4. During May, a cross-equatorial wind from the south Indian Ocean emerged in the low-level (850 hPa) circulation pattern, expanding up to the south AS (Fig. 4a). These cross-equatorial flows intensified throughout the monsoon season, reaching the maximum intensity (> 18 m sec^{-1}) on the Somalian coast and extending to central AS (Fig. 4b). From the AS to the south Indian peninsula, a strong westerly flow can be noticed, which extends to BoB. This clearly shows that the AS delivered essential moisture to the Indian landmass and that a stronger LLJ during the monsoon season boosted precipitation distribution across India in 2020. The strong westerly flow was found from 20

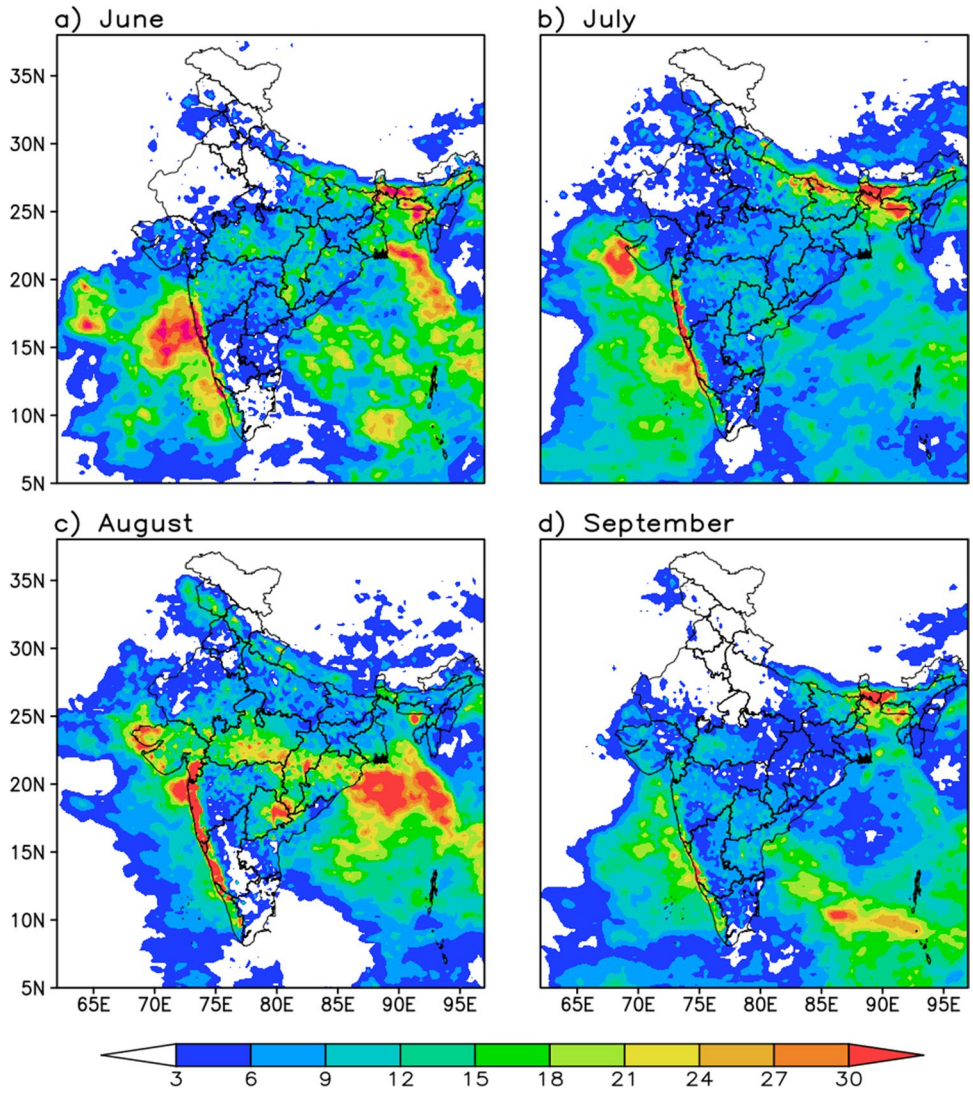

Fig. 2 Observed monthly precipitation during 2020 for **a** June, **b** July, **c** August and **d** September

to 40° N, with a maximum across central-east China, at the upper level (150 hPa) during May (Fig. 4c).

In addition, an anti-cyclonic flow formed over east BoB and continued all the way to the Vietnamese coast. A highly marked and elongated anti-cyclonic flow exists over the Tibet region during the monsoon season (JJAS), which is well represented in the synoptic pattern. A strong extra-tropical westerly flow over the north and a strong tropical easterly flow over the south, with a maximum over the AS, clearly indicated a strong shear pattern on either side of the anti-cyclonic circulation (Fig. 4d).

The temperature and specific humidity distribution (figures not included) at the surface during the pre-monsoon month of May depicts the maximum temperature (> 40 °C) over central to north-west India and the Arabian Peninsula. The zones of maximum temperature decrease over the Indian land mass and increase over Arabian Peninsula during the monsoon season. The predominant cooling was due to the occurrence of precipitation and the release of energy in the monsoon season. The zones of maximum temperature observed the minimum specific humidity. The regions of higher temperature are accompanied by intense convection which plays an important part in the development of heat lows and consequent moisture building over the AS and the Indian Ocean. The oceanic regions have had a higher specific humidity which is due to strong evaporation during the pre-monsoon season. Due to the condensation and subsequent release of latent heat in north-west India, adjoining Pakistan and Arabian Peninsula observed higher temperatures during the monsoon season.

Bias in NCEP forecast

In this section, we analysed the NCEP forecast fields of day 1, day 3, and day 5 respective to the NCEP analysis. The spatial distribution of wind bias at 850 hPa (left panel) and

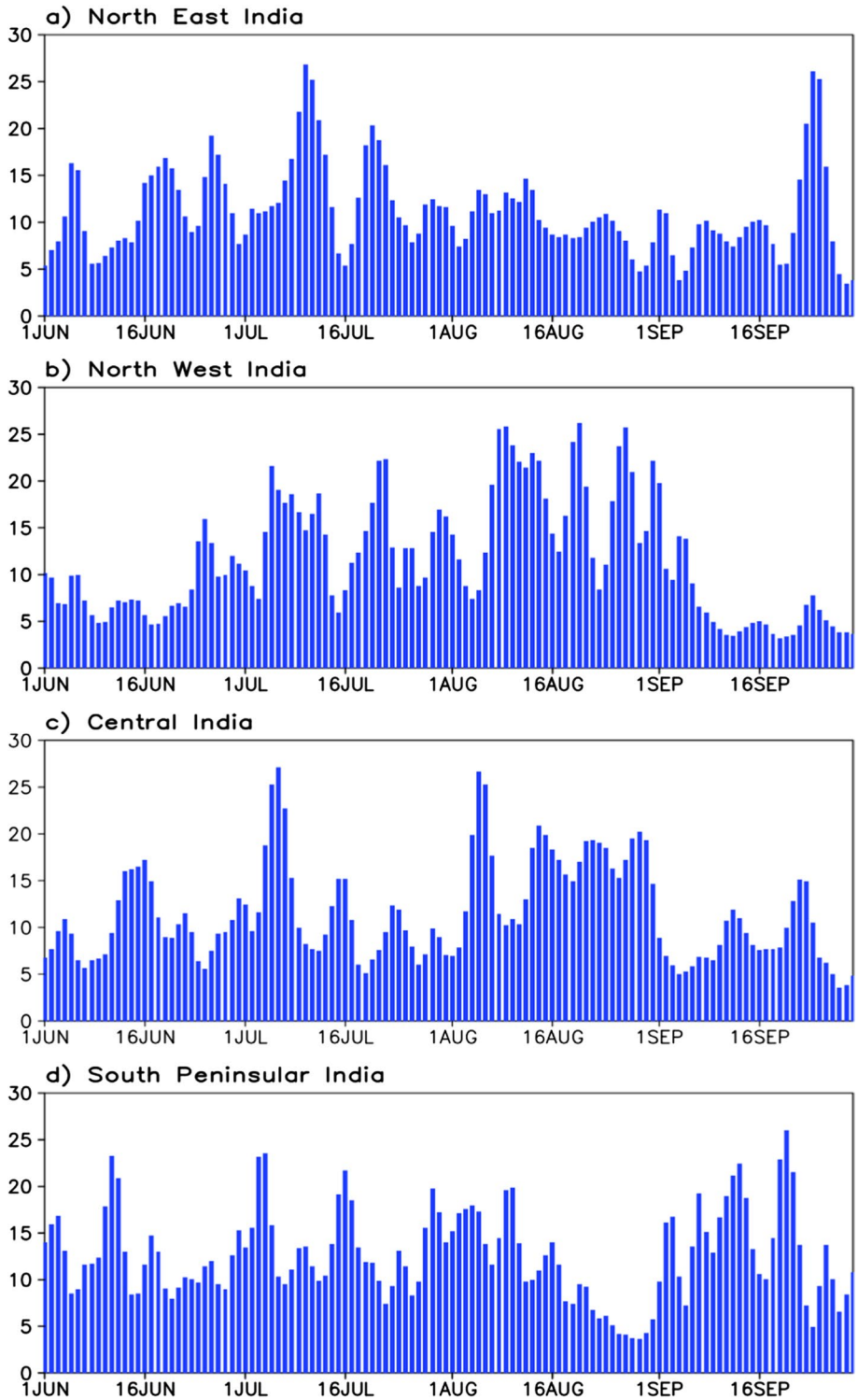

Fig. 3 Observed daily accumulated precipitation during 2020 over four homogeneous regions in India

150 hPa (right panel) for day 1, day 3, and day 5 is presented in Fig. 5. At 850 hPa, there was no wind bias in day 1 analysis (Fig. 5a), indicating that NCEP's day 1 forecast was performing well versus the analysis field. However, forecasts for day 3 and day 5 showed a weaker cross-equatorial flow along the Somalian coast and a strong south-westerly bias over central India, with the most intense over the Gujarat region (Fig. 5c, e). The predictability of low-level synoptic wind features in day 1 forecast is notably well; however, it is decreased with forecast lead time.

Upper-level circulation features (150 hPa) show a positive bias of tropical easterlies in the day 1 forecast, with

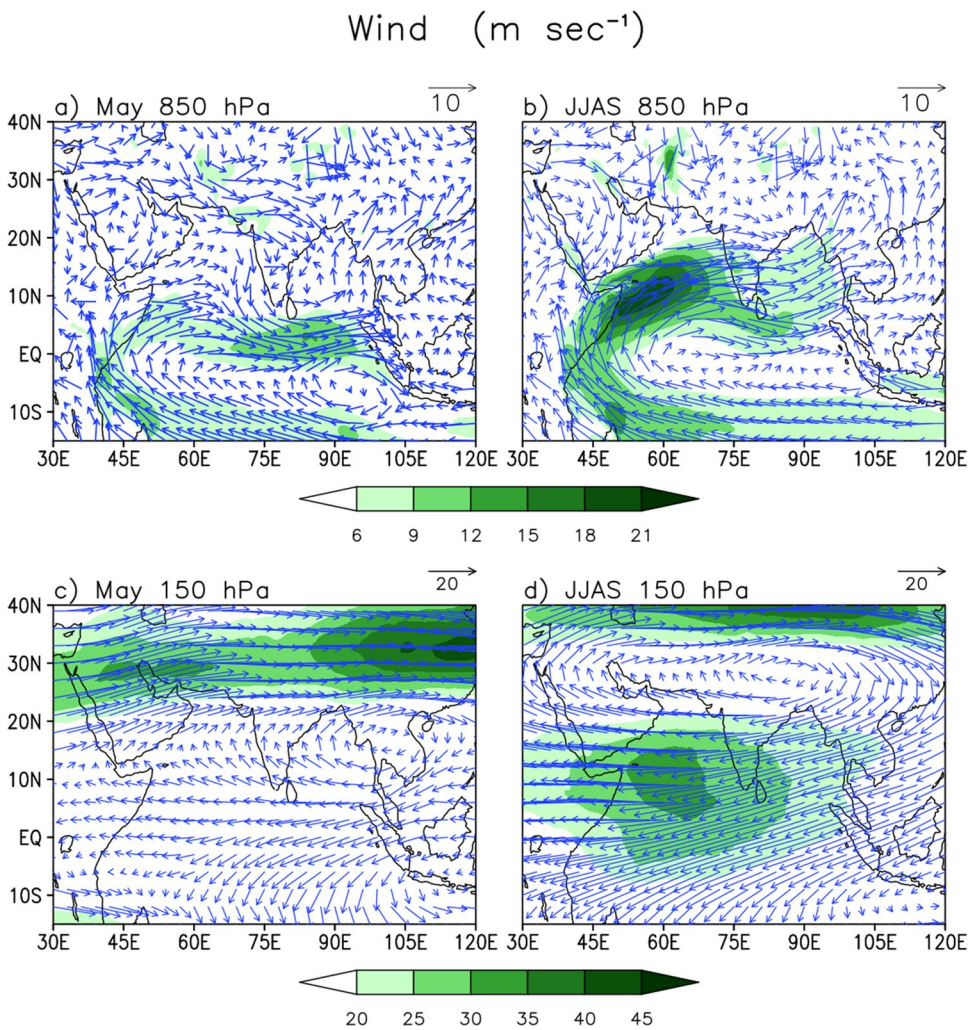

Fig. 4 Spatial distribution wind for **a** May 850 hPa, **b** JJAS 850 hPa, **c** May 150 hPa, **d** JJAS150 hPa

the biasness intensifying over time, indicating a model has a limitation in the upper-level circulation pattern, which could be attributed to the complex topographical terrain. A dipole-type circulation was found with positive bias over the Somalian coast and BoB and negative bias over the Arabian terrain and AS (Fig. 5b). Positive bias at the higher levels intensified as forecast time advanced (Fig. 5d, f). The wind is noted to be distorted due to the change in the circulation pattern, resulting in an anomalous increase in the bias in day 3 and day 5 forecasts.

Spatial distribution of temperature (shaded) and specific humidity (contour) anomalies at 1000 hPa (left panel) and 850 hPa (right panel) for day 1, day 3, and day 5 forecasts are given in Fig. 6. The monsoon trough zone spanning from north-west India up to head Bay had a warm temperature bias in the lower atmosphere (1000 and 850 hPa) with a maximum over north-west India in the day 1, day 3, and day 5 forecasts. The drop in specific humidity in the day 1–5 forecast (Fig. 6) is associated with these zones of warm temperature bias. It was also observed cold bias across the Somalian coast on day 1, day 3, and day 5 forecasts at 1000 and 850 hPa, whereas AS, western and southern India noticed a cold bias in day 3 and day 5 forecasts at 850 hPa which could be due to the intricate topography.

The geopotential height provides information on the warm and cold air masses that are present above the surface (Tomczyk et al. 2019). Because warm air is lighter than cold dense air, the vertical pressure level associated with the cold and warm air masses will be lower and higher, respectively (Cellitti et al. 2006). As a result, the geopotential height is expected to be low in cold air masses and high in warm air masses. The spatial distribution of geopotential height for analysis and bias of day 1, day 3, and day 5 forecasts w.r.t analysis at 850 hPa (left panel) and 200 hPa (right panel) is depicted in Fig. 7. Low geopotential height is noticed over the Himalayan region at 850 hPa (Fig. 7a). In the day 1, day 3, and day 5 forecasts, the forecast field shows that the model has underestimated geopotential height across north-west India and the monsoon trough zone. Higher geopotential height observed

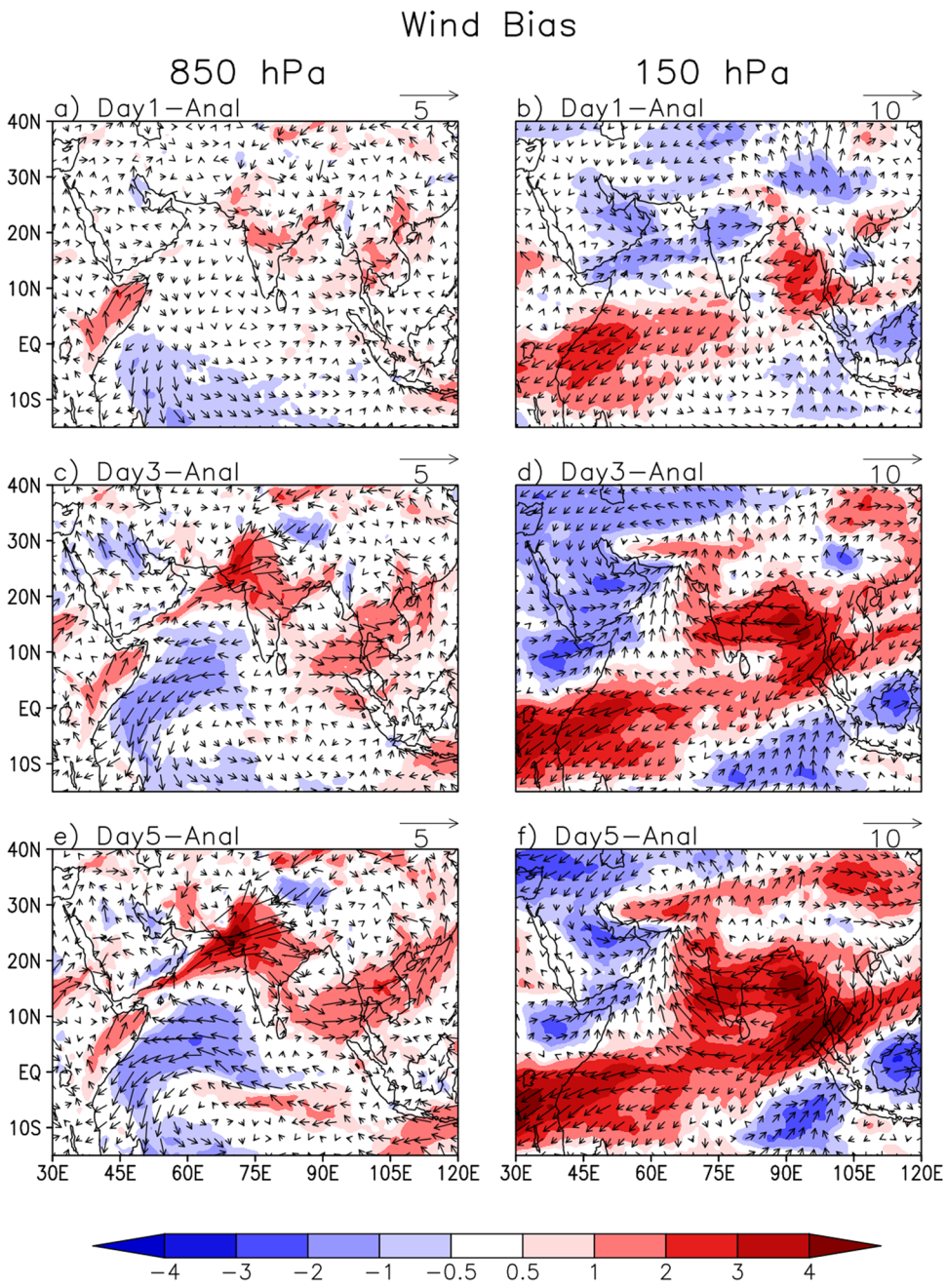

Fig. 5 Spatial distribution of wind bias at 850 hPa (left panel) and 150 hPa (right panel) for **a** and **b** day 1 forecast, **c** and **d** day 3 forecast, **e** and **f** day 5 forecast

over AS w.r.t. analysis. At 200 hPa (Fig. 7, right panel) shows higher geopotential height over Tibetan Plateau, whereas the day 3 and day 5 forecasts show significantly overestimated. Over peninsular India, the geopotential height is underestimated in the forecast of day 1–5.

To examine the model forecasted rainfall, the seasonal rainfall for monsoon 2020 (June–September) for the IMD gridded rainfall and forecast of day 1, day 3, and day 5 is illustrated in Fig. 8. The main contributors to India's monsoonal rainfall being over average (> 9%) in 2020 were excessive rainfall on the west coast, in the central Indian region, and the north-east Indian region. In the year 2020, the monsoon brought less rain to north-western India. The rainfall distribution was well captured in day 1, day 3, and day 5 forecasts, i.e. over the west coast of India, the Indo-Gangetic plain, and the central Indian region. However, the model depicts the wet bias across the central to east-central Indian region and dry bias over the western part of India and a few pockets of north-east India.

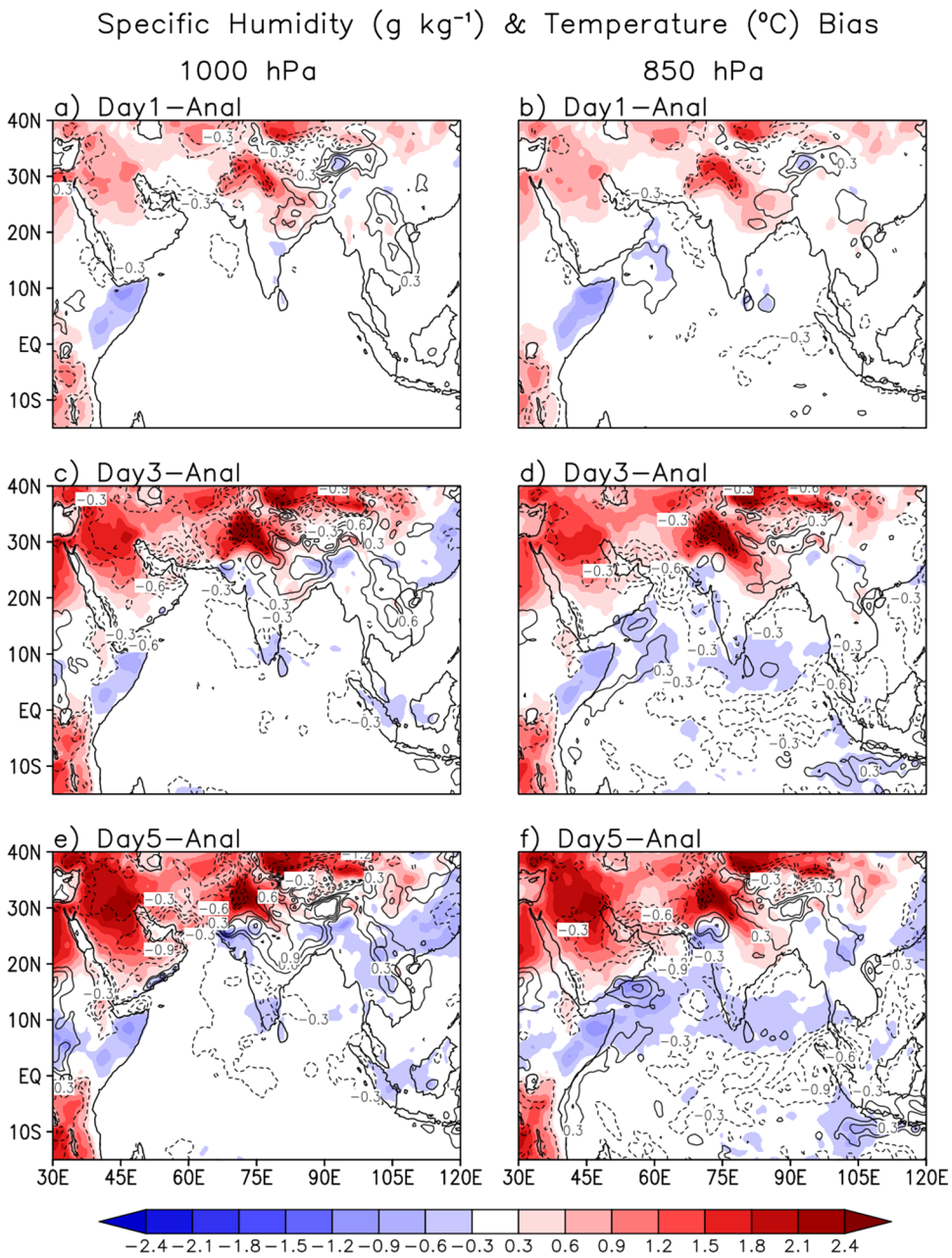

Fig. 6 Spatial distribution of temperature (shaded) and specific humidity (contour) bias at 1000 hPa (left panel) and 850 hPa (right panel) for **a** and **b** day 1 forecast, **c** and **d** day 3 forecast, **e** and **f** day 5 forecast

Extreme weather events

Cyclone Nisarga

Severe cyclone Nisarga increased rainfall activity across India's south-west coast during the monsoon 2020 onset period, as seen in Fig. 2. Severe cyclonic storm Nisarga was the first low-pressure system formed over the AS during the onset of monsoon 2020. Nisarga's evolution began early on May 31st over the east-central AS and Lakshadweep which progressed north-eastwards and made landfall on June 3rd over the Alibaug district of Maharashtra.

Figure 9 depicts 72 h of accumulated precipitation (1–3 June 2020) of IMD gridded rainfall and model forecast of day 1, day 3, and day 5 (top panel) and the corresponding wind distribution at 850 hPa (bottom panel). The rainfall pattern during the cyclonic activity was effectively predicted in the day 1, day 3, and day 5 forecasts. However, the region experienced less intense rainfall as compared to IMD observations. Figure 9e shows a wind pattern (850 hPa) associated with cyclonic movement during the onset of monsoon 2020. There is an intense cross-equatorial flow across the Somalian coast, with strong south-westerlies and well-defined cyclonic circulation over the

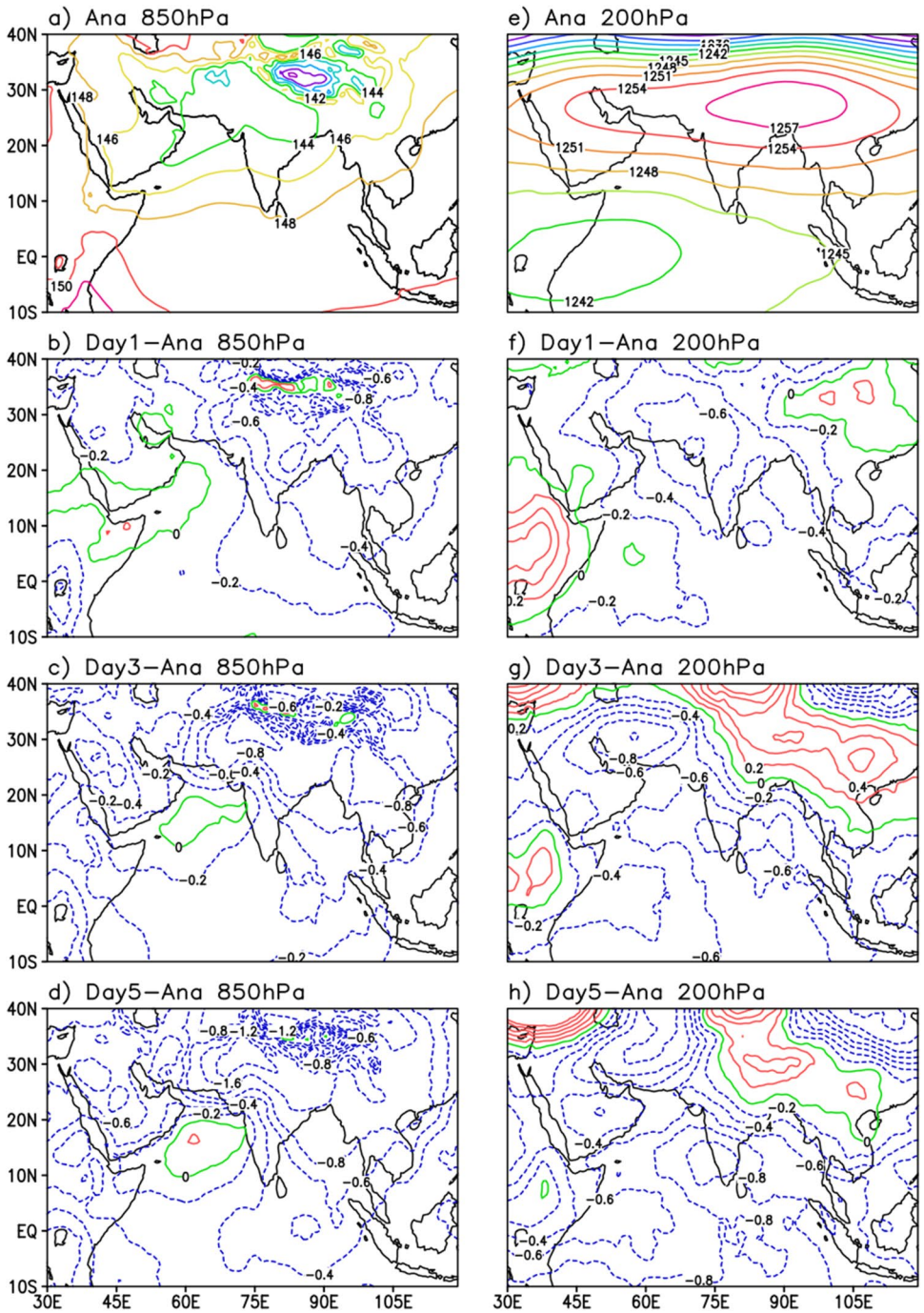

Fig. 7 Spatial distribution of geopotential height at 850 hPa (left panel) and 200 hPa (right panel) for: **a** and **e** analysis, **b** and **f** day 1 bias, **c** and **g** day 3 bias, and **d** and **h** day 5 bias

east-central AS in analysis. Figure 9f–h depicts the forecast fields of 850 hPa wind patterns for day 1, day 3, and day 5. The NCEP model overestimated cross-equatorial flow on day 5, whereas it captured well in the day 1 forecast. In the day 3 forecast, there is weak cross-equatorial flow, and a lack of cyclonic circulation near India's west coast, which led to reduced rainfall over Maharashtra.

Heavy rainfall event

Severe to extreme rainfall events were observed during the active phase of monsoon 2020. Mumbai received heavy rainfall and strong winds from 5 to 6th August 2020 with more than 300 mm of rainfall observed. The high tide waves (3–4 m in height) over AS were observed which restricted the drainage of rainwater to the sea. The public transportation system was disrupted by waterlogging on the roads, rail,

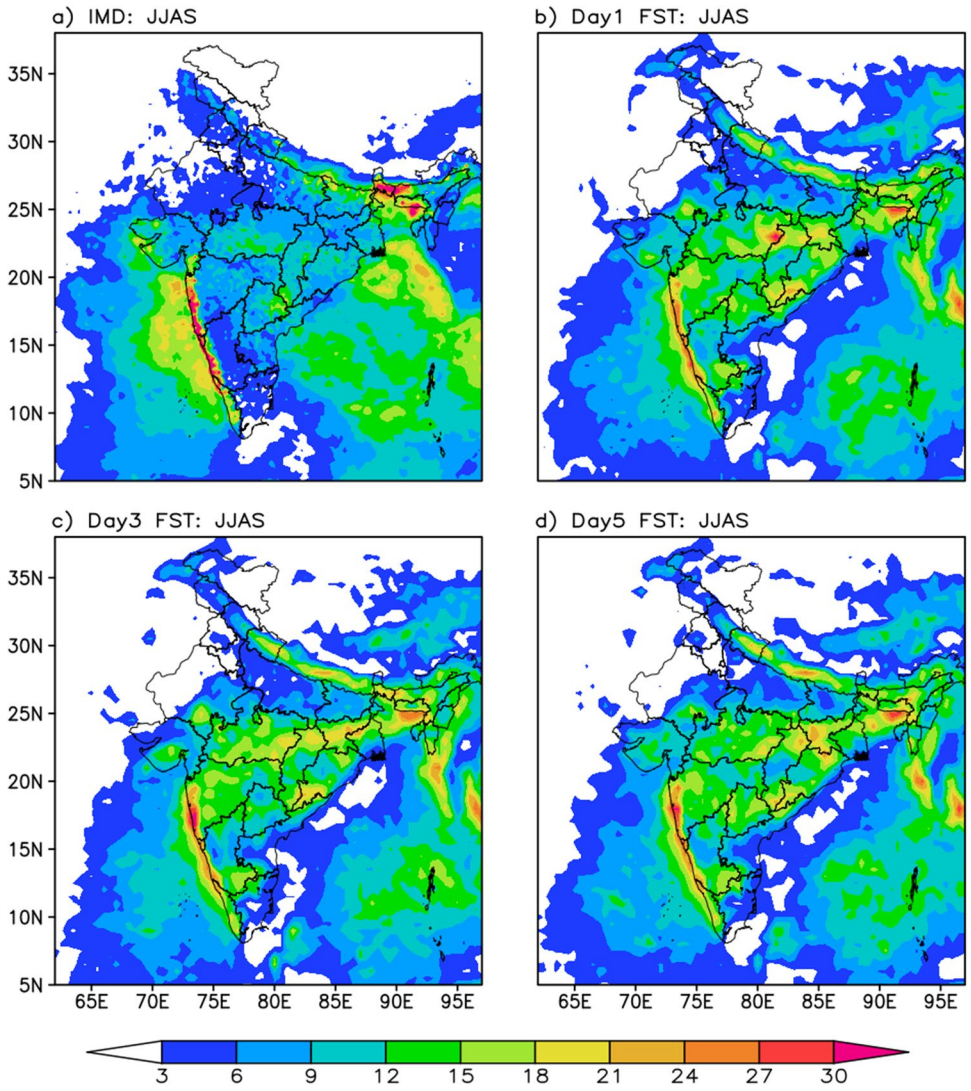

Fig. 8 Spatial distribution of JJAS precipitation for **a** IMD, **b** day 1 forecast, **c** day 3 forecast, and **d** day 5 forecast

and airports. Hence, predicting such rainfall activities in advance is essential and obligatory for the community.

Figure 10 shows the 48-h accumulated rainfall of IMD observations and NCEP model forecasts (5–6th August) and the corresponding wind analysis and forecast fields. Observed rainfall indicates more than 200 mm of rainfall over Mumbai and the south Gujarat region. The spatial pattern of 48 h of accumulated precipitation of day 1 forecast captured the rainfall distribution reasonably well; however, in day 3 and day 5 the model fails to predict the heavy rainfall.

The spatial wind pattern of NCEP analysis at 850 hPa depicts the strong LLJ over AS and also observed a cyclonic circulation centered at Gujarat from 5 to 6th August 2020. A well-defined cross-equatorial flow stretching from Somalia to BoB, with high intensity (> 30 m sec^{-1}) maxima around the central AS could be the main source of moisture transport from the AS to the mainland. Strong westerlies from the Central AS flowing across land regions in southern peninsular India at about 15° N could be a driver of heavy rains in the region (Fig. 10e). The day 1 forecast captured the cross-equatorial wind pattern remarkably well in terms of intensity across the AS (extending up to west BoB), westerlies over the central AS, and cyclonic circulation over Gujarat and Rajasthan (Fig. 10f). The wind intensity around the AS was found to be reduced in the day 3 forecast as compared to the analysis and also observed a northward migration of intensity with south-westerlies over south Gujarat and west Madhya Pradesh. The deficiency of rainfall in day 3 and day 5 forecasts (Fig. 10g, h) is due to a weak LLJ over AS and the absence of cyclonic circulation centered in Gujarat.

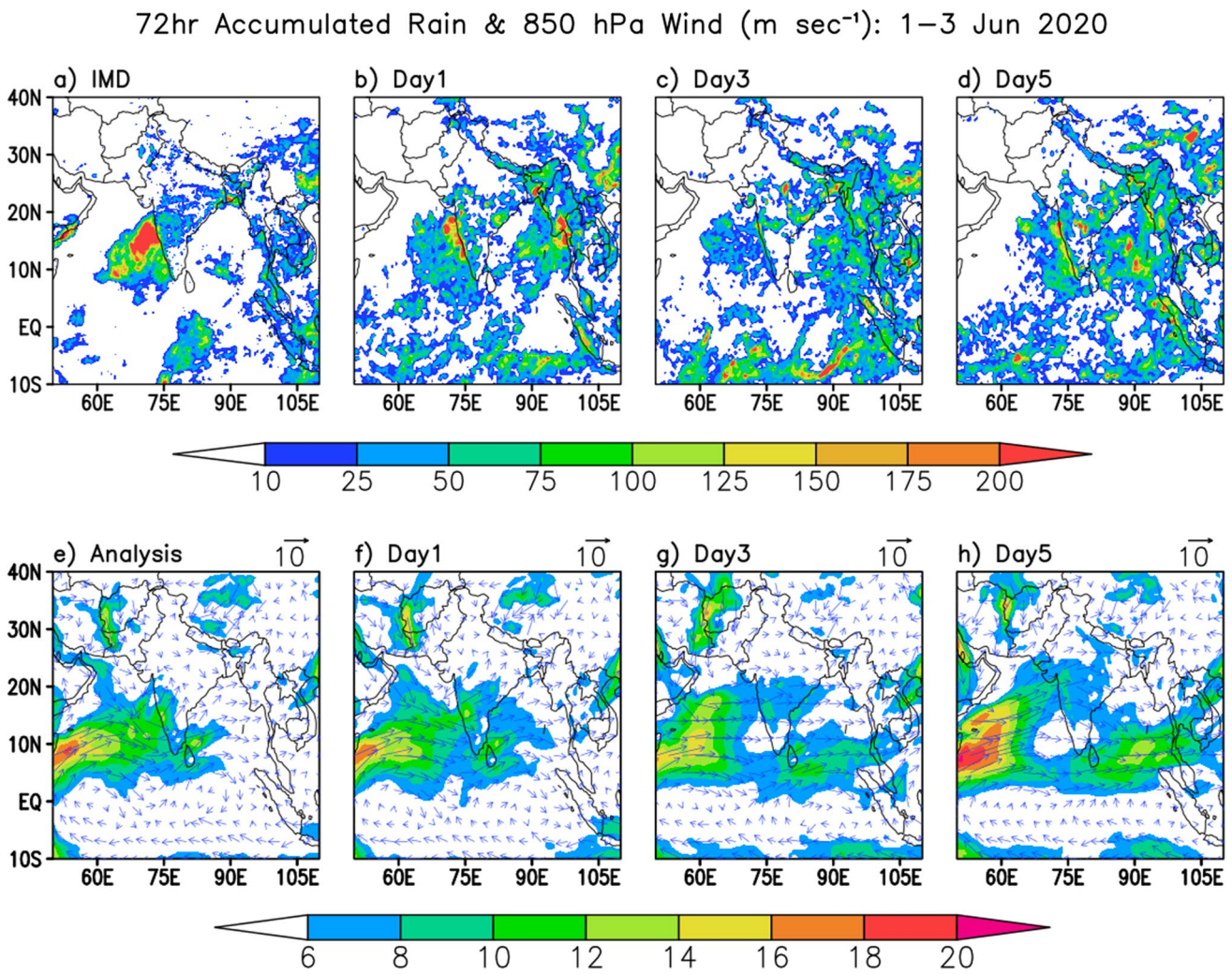

Fig. 9 72 h (1–3 June 2020) accumulated rainfall (top panel) and 850 hPa wind (bottom panel)

Conclusions

The ISM features have been quite reasonably exhibited by NCEP GFS. The seasonal characteristics along with pre-monsoon period also have been discussed. The ISM relevant meteorological parameters such as SST associated with IOD and Nino 3.4 regions, accumulated rainfall, specific humidity, upper and lower circulation patterns, and geopotential height are analysed with respect to respective observation and analysis data.

The analysis of NCEP GFS on ISM 2020 features renders the following broad conclusions:

- The NCEP analysis highlighted semi-permanent characteristics such as low-level westerly flow, upper-level TEJ, heat low in north-western India, and Tibetan high. The model was able to capture these semi-permanent features well in the day 1 forecast; however, the LLJ was found to be feeble at 850 hPa in the day 3 and day 5 forecasts, while the TEJ was noted to be robust.
- In day 1, day 3, and day 5 forecasts, the temperature was noticed to be biased at lower levels (1000 and 850 hPa) over the monsoon trough region extending from north-west India up to the head of Bay. The reduction (increase) of specific humidity in the forecast was associated with areas with warm (cold) temperature bias.
- The spatial distribution of rainfall (IMD gridded rainfall) was in good agreement with day 1, day 3, and day 5 forecasts; however, the intensity was overestimated when compared to IMD observations. In comparison with IMD observation rainfall data, estimated rainfall in the west BoB (around the off-coast Indian region) shows a dry bias in all prediction fields.
- The heavy rainfall events of cyclone Nisarga (1–3 June) over Gujarat and the active phase of the monsoon (5–6 August) over Mumbai which resulted in floods during

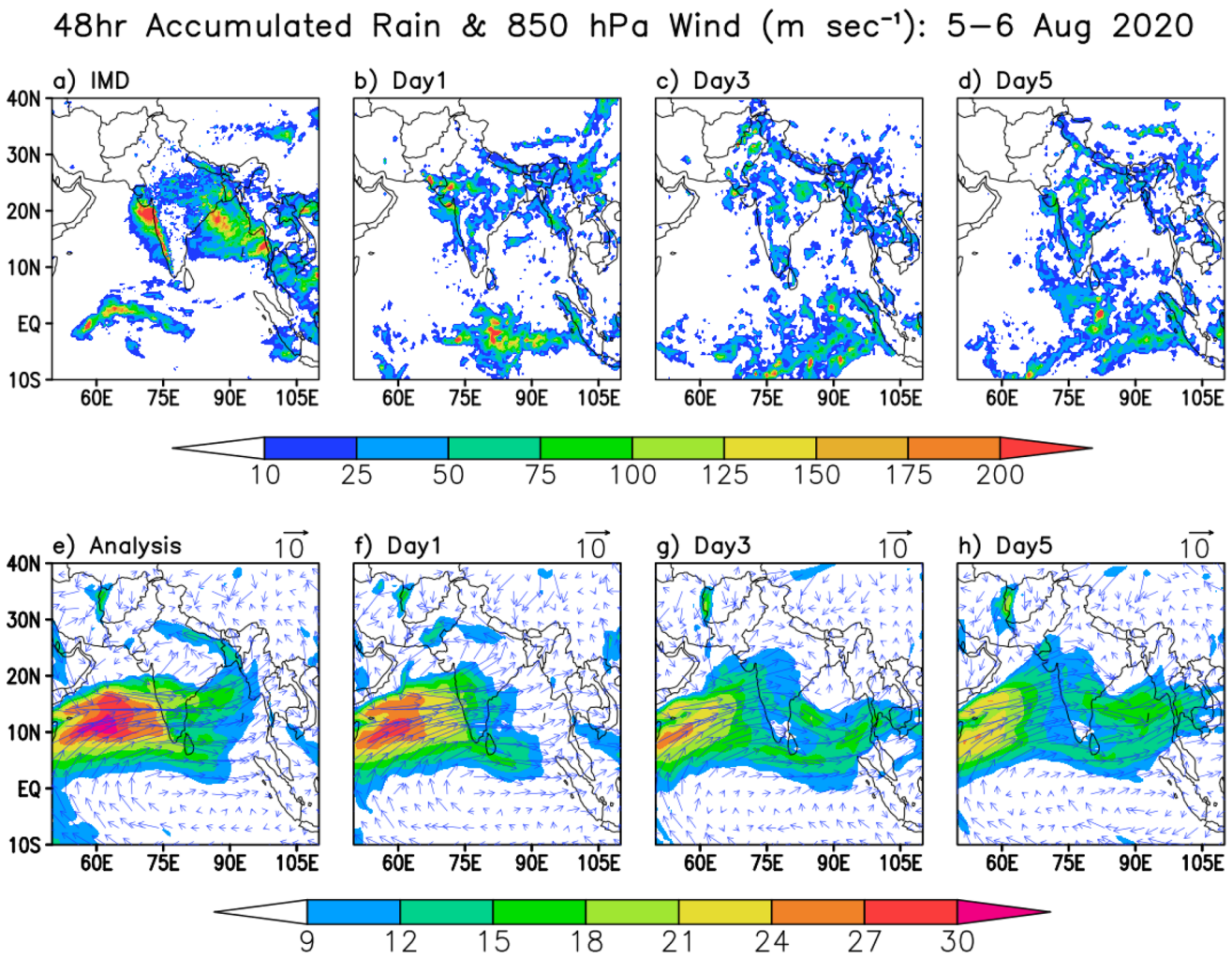

Fig. 10 48 h (5–6 August 2020) accumulated rainfall (top panel) and 850 hPa wind (bottom panel)

the monsoon season was realistically captured in the day 1 forecast in terms of spatial distribution and intensity, but the model has limitation to capture accurate intensity on day 3 and day 5 forecasts.

Acknowledgements The authors acknowledge NCEP for providing analysis and forecast data for the monsoon season 2020 and IMD for providing gridded rainfall data for this study. The current research is funded by a research grant from the Ministry of Earth Sciences (MoES) of the Government of India (MOES/16/11/2016-RDEAS).

Author contributions PVSR contributed to design and conceptualization of the study; AK and MMK contributed to analysis of data and drafting manuscript; and DW contributed to manuscript correction and finalization.

Funding The present work has been carried out under the research grant funded by Ministry of Earth Sciences (MoES), Government of India.

Data availability The datasets generated in this study are available from the corresponding author on request.

Declarations

Conflict of interest On behalf of all authors, the corresponding author states that there is no conflict of interest.

References

Acharya N, Chattopadhyay S, Mohanty UC, Dash SK, Sahoo LN (2012) On the bias correction of general circulation model output for Indian summer monsoon. Meteorol Appl 20:349–356. https://doi.org/10.1002/met.1294

Arpe K, Klinker E (1986) Systematic errors of the ECMWF operational forecasting model in mid-latitudes. Q J R Meteorol Soc 112:181–202. https://doi.org/10.1002/qj.49711146904

Ashfaq M, Cavazos T, Reboita MS, Torres-Alavez JA, Im ES, Olusegun CF, Alves L, Key K, Adeniyi MO, Tall M, Sylla MB, Mehmood S, Zafar Q, Das S, Diallo I, Coppola E, Giorgi F (2021) Robust late twenty-first century shift in the regional monsoons in RegCM-CORDEX simulations. Clim Dyn 57:1463–1488. https://doi.org/10.1007/s00382-020-05306-2

Cellitti MP, Walsh JE, Rauber RM, Portis DH (2006) Extreme cold air outbreaks over the United States, the polar vortex, and the large-scale circulation. J Geophys Res 111:D02114. https://doi.org/10.1029/2005JD006273

DelSole T, Shukla J (2012) Climate models produce skillful predictions of Indian summer monsoon rainfall. Geophys Res Lett 39:L09703. https://doi.org/10.1029/2012GL051279

Gadgil S, Rajeevan M, Nanjundiah R (2005) Monsoon prediction–Why yet another failure? Curr Sci 88:1389–1400

Heckley WA (1985) Systematic errors of the ECMWF operational forecasting model in tropical region. Q J R Meteorol Soc 111:709–738. https://doi.org/10.1002/qj.49711146904

Kalnay E, Kanamitsu M, Kistler R, Collins W, Deaven D, Gandin L, Iredell M, Saha S, White G, Woollen J, Zhu Y, Chelliah M, Ebisuzaki W, Higgins W, Janowiak J, Mo KC, Ropelewski C, Wang J, Leetmaa A, Reynolds R, Jenne R, Joseph D (1996) The NCEP/NCAR 40-year reanalysis project. Bull Am Meteorol Soc 77(3):437–472. https://doi.org/10.1175/1520-0477(1996)077%3c0437:TNYRP%3e2.0.CO;2

Kanamitsu M (1989) Description of the NMC global data assimilation and forecast system. Weather Forecast 4(3):335–342. https://doi.org/10.1175/1520-0434(1989)004%3c0335:DOTNGD%3e2.0.CO;2

Kanamitsu M, Alpert J, Campana K, Caplan P, Deaven D, Iredell M, Katz B, Pan H, Sela J, White G (1991) Recent changes implemented into the global forecast system at NMC. Weather Forecast 6(3):425–435. https://doi.org/10.1175/1520-0434(1991)006%3C0425:RCIITG%3E2.0.CO;2

Karadan MM, Raju PVS, Mishra A (2021) Simulations of Indian summer monsoon using RegCM: a comparison with ERA and GFDL analysis. Theor Appl Climatol 143:1381–1391. https://doi.org/10.1007/s00704-020-03496-7

Krishnan R, Singh B, Vellore R, Mujumdar M, Swapna P, Choudhury A, Rajeevan M (2020) A short perspective on the Mascarene High and the abnormal Indian Monsoon during 2015. Izv Atmos Ocean Phys 4:17–19. https://doi.org/10.48550/arXiv.2011.11372

Kug JS, Sooraj KP, Li T, Jin FF (2010) Precursors of the El Niño/La Niña onset and their inter relationship. J Geophys Re. https://doi.org/10.1029/2009JD012861

Kumar P, Kishtawal CM, Pal PK (2017) Impact of ECMWF, NCEP, and NCMRWF global model analysis on the WRF model forecast over Indian Region. Theor Appl Climatol 127:143–151. https://doi.org/10.1007/s00704-015-1629-1

Lin SJ (2004) A vertically lagrangian finite-volume dynamical core for global models. Mon Weather Rev 132(10):2293–2307. https://doi.org/10.1175/1520-0493(2004)32%3C2293:AVLFDC%3E2.0.CO;2

Mausam E (2021) Weather in India: MONSOON SEASON (June to September 2020). Mausam 72(3):685–718. https://doi.org/10.54302/mausam.v72i3.2979

Mitra A, Bohra A, Rajeevan M, Krishnamurti T (2009) Daily indian precipitation analysis formed from a merge of rain-gauge data with the TRMM TMPA satellite-derived rainfall estimates. J Meteorol Soc Jpn 87A:265–279. https://doi.org/10.2151/jmsj.87A.265

Mohanty UC, Rao PLS, Raju PVS, Bhatla R (2003) A Study of Diagnostic Aspects of South Asian Summer Monsoon. Proc Indian National Sci Acad Part A 69:505–522

Mohanty UC, Raju PVS, Bhatla R (2005) A study on climatological features of the Asian summer monsoon: dynamics, energetics and variability. Pure Appl Geophys 162:1511–1541. https://doi.org/10.1007/s00024-005-2681-z

Pattanaik DR, Kumar A (2010) Prediction of summer monsoon rainfall over India using the NCEP climate forecast system. Clim Dyn 34:557–572. https://doi.org/10.1007/s00382-009-0648-y

Pattanaik DR, Sahai AK, Muralikrishna RP, Mandal R, Dey A (2020) Active-break transitions of monsoons over India as predicted by coupled model ensembles. Pure Appl Geophys 177:4391–4422. https://doi.org/10.1007/s00024-020-02503-2

Patwardhan S, Kulkarni A, Kumar K (2014) Impact of climate change on the characteristics of indian summer monsoon onset. Int J Atmos Sci 201695:11. https://doi.org/10.1155/2014/201695

Pokhrel S, Saha SK, Dhakate A, Rahman H, Chaudhari HS, Salunke K, Hazra A, Sujith K, Sikka DR (2016) Seasonal prediction of Indian summer monsoon rainfall in NCEP CFSv2: forecast and predictability error. Clim Dyn 46:2305–2326. https://doi.org/10.1007/s00382-015-2703-1

Putman WM, Lin SJ (2007) Finite-volume transport on various cubed-sphere grids. J Comput Phys 227(1):55–78. https://doi.org/10.1016/j.jcp.2007.07.022

Raghavan K (1973) Tibetan anticyclone and tropical easterly jet. Pure Appl Geophys 110:2130–2142. https://doi.org/10.1007/BF00876576

Raju PVS, Mohanty UC, Bhatla R (2005) Onset characteristics of the southwest monsoon over India. Int J Climatol 25:167–182. https://doi.org/10.1002/joc.1121

Raju PVS, Mohanty UC, Hsu HH (2010) A study on drought features of the Indian summer monsoon 2002. Meteorol Atmosph Phys 108:43–55. https://doi.org/10.1007/s00703-010-0082-z

Raju PVS, Mishra A, Sundari ABT (2020) Indian summer monsoon features in the NCEP analysis and forecast system. J Earth Syst Sci 129:1–10. https://doi.org/10.1007/s12040-020-01487-w

Raju PVS, Karadan MM, Prasad DH (2022) The role of land surface schemes in non-hydrostatic RegCM on the simulation of Indian summer monsoon. Int J Climatol. https://doi.org/10.1002/joc.7735

Rao PLS, Mohanty UC, Raju PVS, Iyengar G (2003) The Indian summer monsoon as revealed by the NCMRWF system. J Earth Syst Sci 112:95–111. https://doi.org/10.1007/BF02710046

Saha SK, Pokhrel S, Chaudhari HS, Dhakate A, Shewale S, Sabeerali CT, Salunke K, Hazra A, Mahapatra S, Rao AS (2014) Improved simulation of Indian summer monsoon in latest NCEP climate forecast system free run. Int J Climatol 34:1628–1641. https://doi.org/10.1002/joc.3791

Tomczyk AM, Sulikowska A, Bednorz E, Półrolniczak M (2019) Atmospheric circulation conditions during winter warm spells in Central Europe. Nat Haz 96(3):1413–1428. https://doi.org/10.1007/s11069-019-03621-4

Wang B, Ding Q, Fu X, Kang IS, Jin K, Shukla J, Doblas-Reyes F (2005) Fundamental challenge in simulation and prediction of summer monsoon rainfall. Geophys Res Lett 32:L15711. https://doi.org/10.1029/2005GL022734

Wang B, Ding Q, Joseph PV (2009) Objective definition of the Indian summer monsoon onset. J Clim 22:3303–3316. https://doi.org/10.1175/2008JCLI2675.1

Wang Z, Li G, Yang S (2018) Origin of Indian summer monsoon rainfall biases in CMIP5 multimodel ensemble. Clim Dyn 51:755–768. https://doi.org/10.1007/s00382-017-3953-x

Webster PJ, Magana VO, Palmer TN, Shukla J, Tomas RA, Yanai MU, Yasunari T (1998) Monsoons: processes, predictability, and the prospects for prediction. J Geophys Res Oceans 103:14451–14510. https://doi.org/10.1038/43848